



# Effect of Cooling Rate on Microstructure and Hardness during Solution Treatment and Aging Process of Ti-6Al-4V Alloy for Aerospace Components

Seongji Seo, Hojoon Choi, Geeyoung Lee, Kee-Ahn Lee, Jeongho Han, and Minsu Jung

Submitted: 26 May 2020 / Revised: 4 February 2021 / Accepted: 14 February 2021 / Published online: 26 March 2021

The microstructure and hardness of Ti-6Al-4V alloys were evaluated before and after aging to investigate the effect of the cooling rate at the solution treatment stage of the solution treatment and aging (STA) process for aerospace components. The cooling rate distribution across a Ti-6Al-4V alloy sample representing practical STA process of an aerospace fan disk component was estimated using finite element analysis. The Ti-6Al-4V alloy specimens were solution-treated with the obtained cooling rates, and aged. Experimental WQ of the Ti-6Al-4V alloy specimen in the solution treatment facilitated the retention of the primary  $\alpha$  phase, while the  $\beta$  phase was transformed to  $\alpha'$ . Controlled cooling at slower rates compared to WQ led to the formation of coarser globular  $\alpha$  and the transformation of  $\beta$  to  $\alpha+\beta$  lamellae. Subsequent aging of the specimens led to the observation of  $\alpha+\beta$  lamellae in all specimens regardless of the cooling conditions, where the average thickness of the plates in lamellae was higher at slower cooling rates. The specimens exhibited higher hardness values when cooled more quickly at the solution treatment, which was attributed to the formation of thinner  $\alpha$  plates and/or a higher  $\alpha'$  fraction. The hardness value of all specimens increased further after aging, regardless of the cooling conditions, due to precipitation of  $Ti_3Al$  in the  $\alpha$  phase and/or fine  $\alpha$  plates from the  $\alpha'$  phase.

**Keywords** cooling rate, hardness, microstructure, solution treatment and aging, Ti-6Al-4V

## 1. Introduction

Titanium (Ti) alloys are widely used in various industries such as aerospace, military and petrochemicals due to their excellent specific strength, corrosion resistance and high temperature properties (Ref 1–4). In particular, Ti-6Al-4V alloy is commonly used in aerospace industry for structural as well as engine components such as fan blades, disks, shafts owing to not only the above-mentioned properties, but also outstanding combination of strength and ductility (Ref 4).

Ti-6Al-4V alloy generally consists of alpha ( $\alpha$ ) and beta ( $\beta$ ) phases, and the mechanical properties can be controlled by adjusting the microstructure via heat treatments such as mill-annealing or solution treatment and aging (STA) (Ref 4). STA

typically leads to a  $\sim 20\%$  higher tensile strength than that from mill-annealing (Ref 5). Further, since STA heat treatment also gives to proper ductility, it is often used to improve the mechanical properties of aerospace components.

In the process of manufacturing aerospace components of Ti-6Al-4V alloy, STA heat treatment is performed according to the AMS 4965 standard. This procedure involves solution treatment of the component by heating to 954 °C ( $\pm 14$  °C) with an isothermal hold for 1 to 2 h, followed by water quenching (WQ). The component is subsequently aged by heating to a temperature between 482 and 621 °C with an isothermal hold for 4 to 8 h, followed by air cooling (AC) (Ref 6). The thermal conductivity of Ti-6Al-4V is typically poor, thus a large aerospace component can exhibit significantly different cooling rates at its surface and interior during WQ in the solution treatment. This difference in cooling rate can lead to differences in the microstructure and mechanical properties of the different parts of the component after solution treatment, as well as after aging.

The microstructure and mechanical properties of Ti-6Al-4V have been previously investigated under various cooling conditions in the solution treatment stage of STA heat treatment (Ref 7–19). Studies on the effects of cooling rate during solution treatment have revealed that WQ after isothermal holding leads to the transformation of  $\beta$  to  $\alpha'$ , while gradual cooling at a slower rate leads to the transformation of  $\beta$  to  $\alpha+\beta$  lamellae and, in turn, a decrease in hardness (Ref 7–9). Further, when aging after WQ,  $\alpha'$  is transformed into  $\alpha + \beta$  (Ref 10–14), while aging after relatively slow cooling, each plate of lamellae already formed becomes much coarser (Ref 15–17). Similarly, the hardness after aging is lower when lower cooling rate used in solution treatment (Ref 17). Morita et al. (Ref 12) reported that the precipitation of fine  $\alpha$  phases during aging can improve the tensile strength and yield strength of water-quenched Ti-

**Seongji Seo**, Intelligent Manufacturing R&D Department, Korea Institute of Industrial Technology, Siheung 15014, Korea; and Department of Materials Science and Engineering, Hanyang University, Seoul 04763, Korea; **Hojoon Choi**, Shape Manufacturing R&D Department, Korea Institute of Industrial Technology, Songdo 21999, Korea; **Geeyoung Lee**, KPC Metal Co., Ltd., Gyeongsan 38412, Korea; **Kee-Ahn Lee**, Department of Materials Science and Engineering, Inha University, Incheon 22212, Korea; **Jeongho Han**, Department of Materials Science and Engineering, Hanyang University, Seoul 04763, Korea; and **Minsu Jung**, Intelligent Manufacturing R&D Department, Korea Institute of Industrial Technology, Siheung 15014, Korea. Contact e-mail: mjung@kitech.re.kr.

6Al-4V in solution treatment. Lin et al. (Ref 15) found that as the aging temperature increases, the secondary phases grow and extend into the equiaxed  $\alpha$  phase, and merge to form a new curved lamellar phase, by analyzing Ti-6Al-4V alloys which were air-cooled in solution treatment and aged at various temperatures. Pinke et al. (Ref 17) mentioned the phase transformations and hardness change during STA heat treatment according to the cooling conditions (WQ and AC) during solution treatment, but explanation for the correlation between the hardness change and the microstructure is insufficient. Gupta et al. (Ref 18) and Ren et al. (Ref 19) investigated microstructure and mechanical properties after aging in terms of the cooling rates of solution treatment in STA heat treatment, as ‘WQ versus AC’ and ‘WQ versus AC versus furnace cooling (FC),’ respectively. However, the samples in these studies (Ref 18, 19) were only analyzed after the subsequent aging step, not immediately after solution treatment.

The findings of these previous studies (Ref 7-19) provide insights to resolve the issues associated with irregular cooling rate distribution across larger aerospace components during solution treatment according to the AMS 4965 standard. Among the various cooling conditions, namely WQ, AC, and FC, WQ correspond to the cooling rate of the surface of the component, while AC and FC are typically slower than the cooling rate of the core of the component. Thus, these cooling conditions do not truly represent the cooling rate distribution of an aerospace component, nor the resulting changes in microstructure and hardness.

Therefore, in this study, when WQ of Ti-6Al-4V alloy of approximate size of an aerospace fan disk component in solution treatment process according to AMS 4965 standard, the distribution of cooling rate in the sample was predicted using finite element analysis. Afterward, changes in microstructure and hardness with the predicted cooling rates during STA were quantitatively investigated by experimentally controlling the cooling rates within the entire range of the component using a dilatometer. The microstructural changes observed at the different cooling rates were thoroughly evaluated via phase transformation analysis and phase fraction calculations based on optical microscopy (OM), field-emission scanning electron microscopy (FE-SEM), and x-ray diffraction (XRD). Furthermore, the relationship between the microstructure and hardness changes according to cooling rate was clarified.

## 2. Experimental

### 2.1 Material

A Rod-shaped Ti-6Al-4V alloy sample ( $\varnothing 70 \times 2000$  mm) fabricated via vacuum arc remelting (VAR) and rotary-forging were obtained from KPCM Co., Ltd., where the chemical

**Table 1 Chemical composition (wt.%) of Ti-6Al-4V alloy used in this study**

Ti	Al	V	Fe	O	N	C	H
Balance	6.56	4.15	0.19	0.19	0.021	0.027	0.003

composition is given in Table 1. The sample was mill-annealed for 2 h at 705 °C, followed by air cooling.

### 2.2 Determination of Cooling Rate Conditions by Finite Element Analysis

Heat treatment finite element analysis software (DEFORM-HT3) was used to analyze heat transfer during WQ after isothermal holding at 950 °C for 1 h. A disk-shaped Ti-6Al-4V alloy sample ( $\varnothing 600 \times 200$  mm) with a similar size to an aerospace fan disk component was used. Due to the symmetry, 1/12 of the disk-shaped sample was modeled using 30081 tetrahedral elements with 6782 nodes. The initial temperature was set to 950 °C for all nodes, and the heat transfer coefficient for WQ was taken as 5 kW/m<sup>2</sup>°C. The cooling rates of the sample core (P1), intermediate point (P2), and surface (P3) were 0.4, 0.8, and 133.8 °C/s, respectively (Fig. 1). Table 2 shows the calculated phase fraction after cooling to room temperature at the predicted cooling rates from the equilibrium state of 950 °C were simulated using JMatPro software (Ref 20). The samples cooled at 0.4 and 0.8 °C/s exhibited similar amounts of  $\alpha$  and  $\beta$  phases, which indicated the amounts and types of phases formed at cooling rates below 1 °C/s were similar. However, a cooling rate of 133.8 °C/s was sufficiently rapid to transform the existing  $\beta$  phase to the  $\alpha'$  phase. Therefore, it was intended to investigate microstructure changes when cooled at cooling rates between 1 and 133.8 °C/s and WQ (i.e., fastest rate). Based on these analysis, the microstructure and hardness changes at cooling rates of 1, 10, 50 °C/s, and WQ after isothermal holding during solution treatment were investigated experimentally.

### 2.3 Heat Treatments

The specimens were machined to give smaller rod-shaped specimens ( $\varnothing 3 \times 10$  mm), thereby minimizing the mass effect during cooling. The specimens were isothermally held at 950 °C for 1 h and cooled either at controlled rates or WQ. Controlled cooling was conducted to 1, 10, or 50 °C/s under vacuum ( $4 \times 10^{-4}$  torr) in a dilatometer (Dilatronic III, Theta Industries). The error of the cooling rate measured is level of 0.01 °C/s. In the case of WQ, it was performed under vacuum ( $6 \times 10^{-4}$  torr) in a quartz furnace. All cooled specimens were aged with a isothermal hold at 500 °C for 4 h under vacuum ( $6 \times 10^{-4}$  torr) in a quartz furnace, followed by air cooling (Fig. 2).

### 2.4 Characterization

The heat-treated specimens were polished using a 1  $\mu$ m diamond suspension after general mechanical polishing, and finally, oxide polishing was performed using OP-S solution. The specimens were etched using Kroll’s reagent comprising HF (2%) and HNO<sub>3</sub> (3%) in distilled H<sub>2</sub>O (95%) before observing the surface microstructure in the transverse direction using an optical microscope (OM, HRM-300, Huvitz) and a field emission-scanning electron microscope (FE-SEM, NNS-450, FEI). The globular  $\alpha$  phase fraction in the OM images was measured using I-solution DT software, while the thickness of the  $\alpha$  plates in the lamellar phase and  $\alpha'$  plates were determined from the scanning electron microscope (SEM) images.

X-ray diffraction (XRD, X’pert-PRO MPD, PANalytical) analysis was performed in a  $2\theta$  range of 30° to 90° at a scan rate of 0.02° min<sup>-1</sup> (x-ray: Cu K $\alpha$ ). The phase fractions were

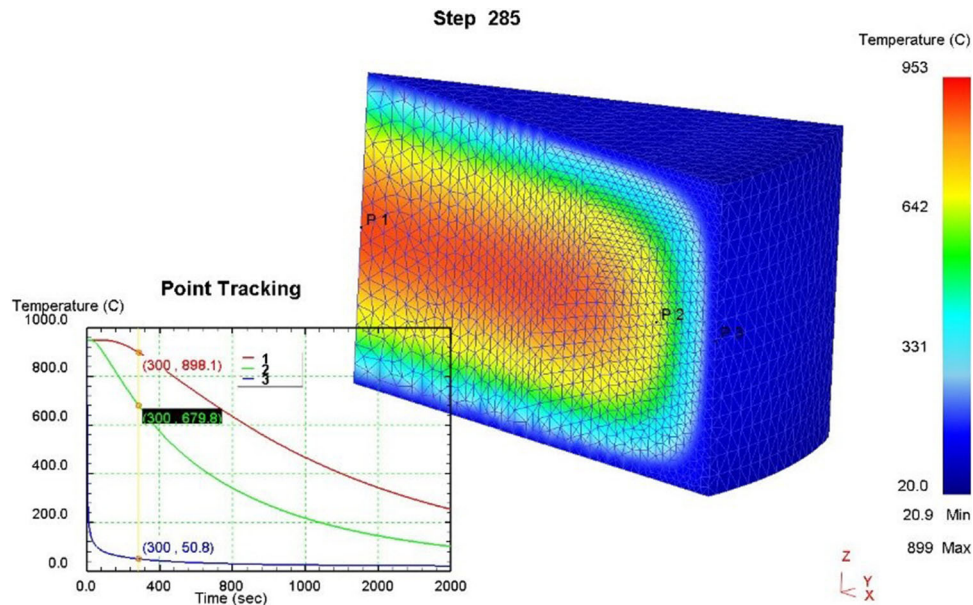


Fig. 1 Heat transfer analysis for WQ cooling of the approximate size of an aerospace fan disk component of Ti-6Al-4V alloy after isothermal holding at from 950 °C

Table 2 Phase fractions (at.%) after cooling at 0.4, 0.8, 133.8 °C/s from an equilibrium state of 950 °C, calculated by JMatPro (Ref 20)

	0.4, °C/s	0.8, °C/s	133.8, °C/s
$\alpha'$	...	...	68.78
$\alpha$	93.49	92.43	31.22
$\beta$	6.51	7.57	...

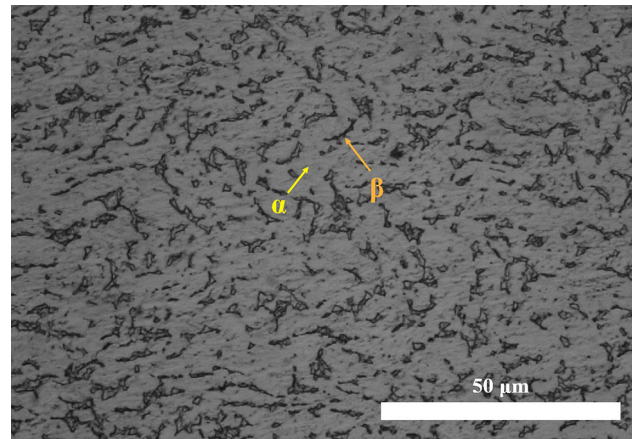


Fig. 3 OM image showing microstructure of a mill-annealed Ti-6Al-4V round bar

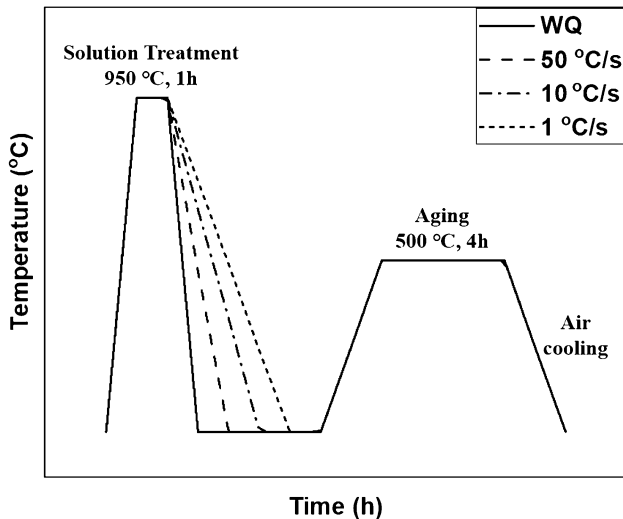


Fig. 2 Heat treatment conditions used for the STA processing in this study

calculated based on the ratio of the integral intensity of the peaks in the XRD patterns (Ref 21).

To find out the changes in hardness during the STA process when the cooling rates of the solution treatment process were

different, the hardness values were measured with a load of 1 kgf by using a micro-Vickers hardness tester (HM-210 B, Mitutoyo).

### 3. Results and Discussion

#### 3.1 Microstructure

The OM image of the as-received Ti-6Al-4V alloy (transverse direction) reveals a microstructure consisting of equiaxed  $\alpha$  phase with  $\beta$  phase. The  $\beta$  phase have settled along the grain boundaries of the  $\alpha$  phase (Fig. 3). The OM and SEM micrographs of the specimens cooled at controlled cooling rates (1, 10, and 50 °C/s) and via WQ during solution treatment are given in Fig. 4(a), (b), (c), (d), (e), and (f). Overall, they show a bimodal (duplex) microstructure comprising globular  $\alpha$  phase and  $\alpha + \beta$  lamellar or  $\alpha'$  phase (Ref 16), and a very small



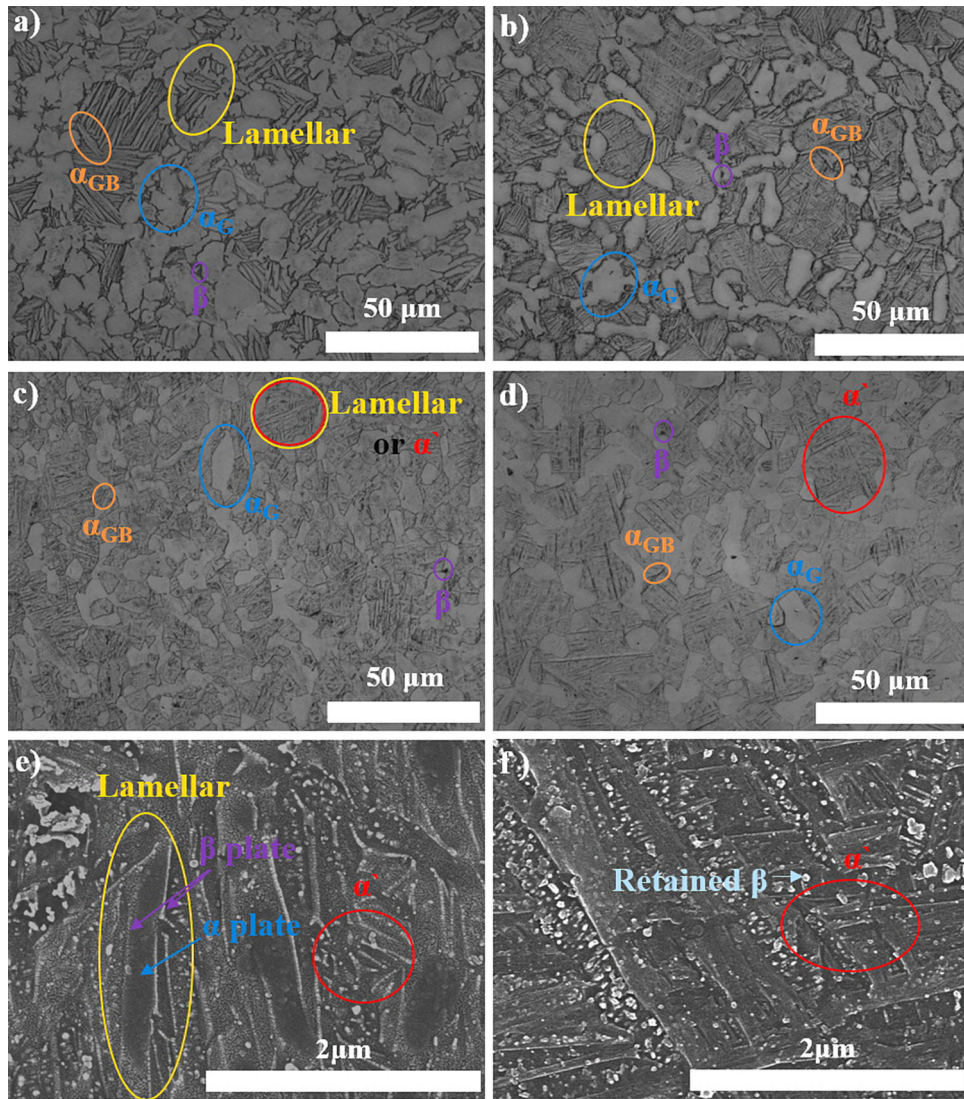


**Fig. 4** OM images of Ti-6Al-4V alloys after solution treatment with different cooling rates of (a) 1 °C/s, (b) 10 °C/s, (c) 50 °C/s, and (d) WQ; SEM micrographs of the transformed  $\beta$  phase after cooling at (e) 50 °C/s and (f) WQ

amount of retained  $\beta$  phase within the specimens. The specimens isothermally held at 950 °C and cooled via WQ exhibit a globular  $\alpha$  phase ( $\alpha_G$ ) with a similar size to the primary  $\alpha$  phase ( $\alpha_P$ ). However, the specimens cooled at controlled cooling rates of 1 to 50 °C/s exhibit coarsening of  $\alpha_G$  as the cooling rate became slower (Fig. 4a, b, and c). The grain boundary  $\alpha$  phase ( $\alpha_{GB}$ ) also becomes coarser at slower cooling rates, where  $\alpha_{GB}$  grows to a size similar to  $\alpha_G$  at 1 °C/s (Fig. 4a).

WQ is rapid enough to facilitate the transformation of  $\beta$  to  $\alpha'$ , as observed in the OM image (Fig. 4d). However, the  $\alpha + \beta$  lamellae and  $\alpha'$  formed in the specimen cooled at 50 °C/s were not easily distinguished in the OM image (Fig. 4c). Thus, the transformed  $\beta$  phase was analyzed at high magnification using SEM (Fig. 4e), which confirmed that cooling at 50 °C/s leads to the formation of both  $\alpha'$  and  $\alpha + \beta$  lamellae which consists of the dark-colored  $\alpha$  plates and the bright-colored  $\beta$  plates in the transformed  $\beta$  phase. The SEM micrograph of the specimen cooled via WQ (Fig. 4f) exhibits predominant acicular  $\alpha'$  surrounded by the retained  $\beta$  phase.

OM and SEM micrographs of the aged specimens (500 °C for 4 h) cooled at 1, 10, and 50 °C/s and via WQ during solution treatment reveal that all specimens comprise a bimodal (duplex) microstructure similar to that observed before aging (Fig. 5a, b, c, d, e, and f). However, the SEM micrographs reveal that the  $\alpha + \beta$  lamellae consists of fine  $\alpha$  and  $\beta$  plates decomposed from the  $\alpha'$  phase (Fig. 5e and f), (Ref 15). A slower cooling rate leads to more coarsening of  $\alpha_G$  and  $\alpha_{GB}$  during aging, where the slowest cooling conditions of 1 °C/s leads to very coarse  $\alpha_G$  and  $\alpha_{GB}$  and, in turn, large fractions of  $\alpha_G$  and  $\alpha_{GB}$  (Fig. 5a). The  $\alpha$  plates inside the  $\alpha + \beta$  lamellae also tend to coarsen during aging when a slower cooling rate was used. However, the SEM micrographs of the aged specimens cooled at 50 °C/s and via WQ during solution treatment reveal that  $\alpha'$  was transformed to  $\alpha + \beta$  lamellae (Fig. 5e and f). Further, fine spherical particles are scattered within the  $\alpha$  phase in some areas, which is attributed to precipitated  $Ti_3Al$  phases. A time–temperature–transformation (TTT) curve was produced using JMatPro (Ref 20), which reveals that the precipitation of  $Ti_3Al$  at 500 °C initiated at 5545 s (93 min) (Fig. 6). Therefore,

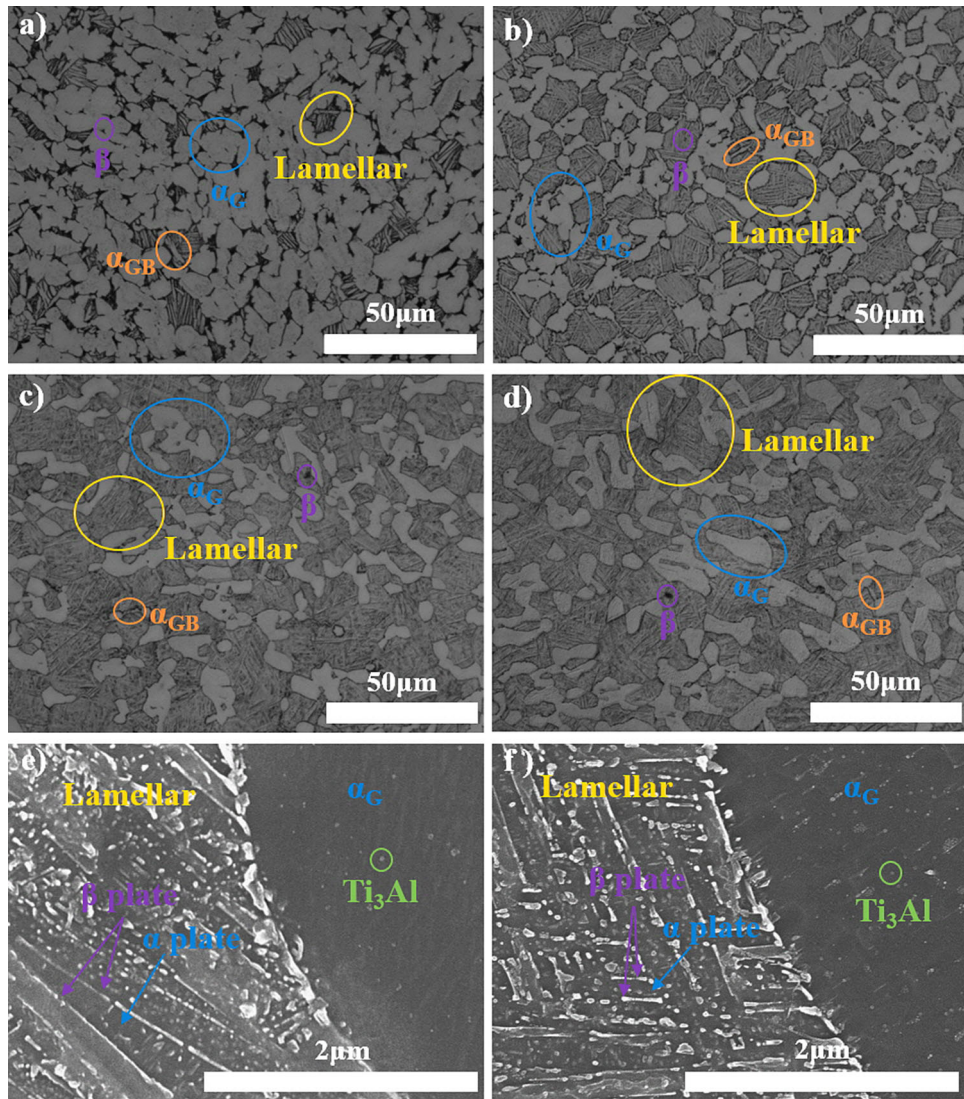


**Fig. 5** OM images of Ti-6Al-4V alloys after subsequent aging at 500 °C for 4 h after solution treatment with different cooling rates of (a) 1 °C/s, (b) 10 °C/s, (c) 50 °C/s, and (d) WQ; SEM micrographs of the  $\alpha + \beta$  lamellar phase and  $\alpha_G$  phase, including  $Ti_3Al$  precipitates after cooling at (e) 50 °C/s and (f) WQ

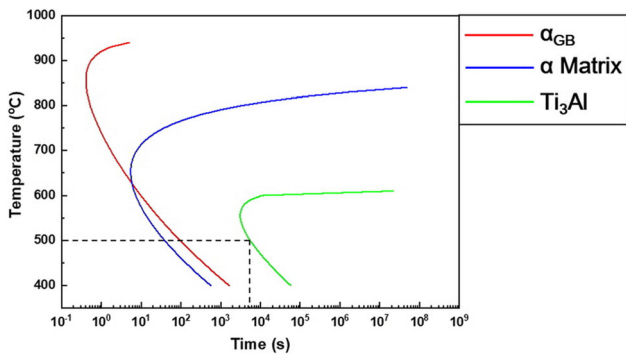


**Fig. 6** TTT diagram of the phases in the Ti-6Al-4V alloy used in this study by using JMatPro (Ref 20)

aging at 500 °C for 4 h in this study allows for sufficient  $Ti_3Al$  nucleation and growth.

### 3.2 X-Ray Diffraction and Phase Fraction

XRD analysis of the specimens cooled at 1, 10, and 50 °C/s and via WQ during solution treatment was compared to the indexed results for diffraction peaks given in Inorganic Crystal Structure Database (ICSD) cards. The specimens comprise  $\alpha$ -Ti (ICSD 98-007-6265),  $\beta$ -Ti (ICSD 98-007-6165), and  $\omega$ -Ti (ICSD 98-015-0817) phases (Fig. 7). Cooling via WQ leads to peaks corresponding to the  $\beta$  phase due to the presence of retained  $\beta$  phase that was not transformed to  $\alpha'$ , as observed in the OM and SEM images (Fig. 4d and f). The peaks attributed to  $\alpha$  and  $\alpha'$  are difficult to distinguish because  $\alpha$  and  $\alpha'$  have the same crystal structure (hcp) and a very similar lattice parameter (Ref 13).

The specimens cooled at 50 °C/s and via WQ both exhibit peaks attributed to a small amount of the athermal  $\omega$  phase, which is a metastable phase formed when a  $\beta$  phase with sufficient  $\beta$ -stabilizing elements undergoes rapid cooling (Ref 10, 22). The calculated amount of V, which serves as a  $\beta$ -stabilizing element in the  $\beta$  phase, in the Ti-6Al-4V alloy in



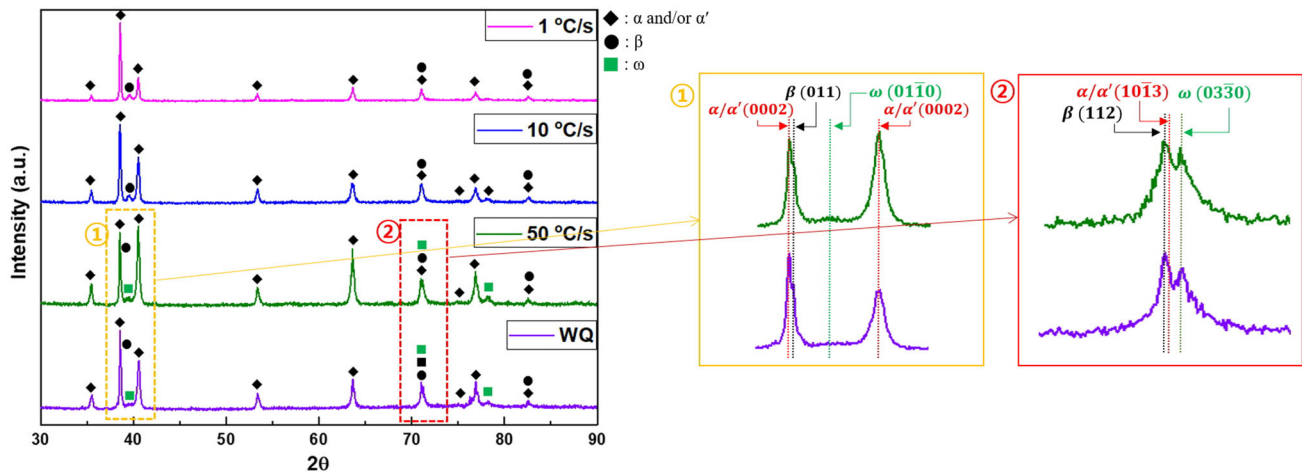


Fig. 7 XRD patterns of Ti-6Al-4V alloys after solution treatment with different cooling rates

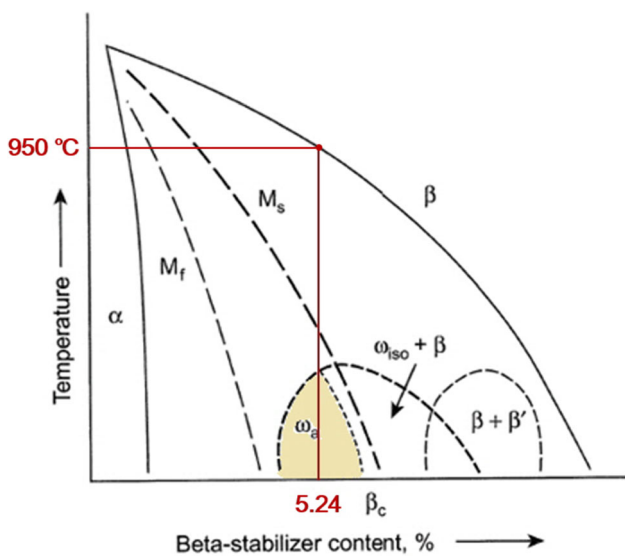


Fig. 8 Schematic phase diagram of titanium alloys (Ref 10), where the equilibrium V content in  $\beta$  phase at 950 °C for Ti-6Al-4V alloy used in this study is indicated

equilibrium at 950 °C is determined as 5.24 wt.% using JMatPro (Ref 20). Rapid cooling of this  $\beta$  phase with 5.24 wt.% V leads to the formation of  $\omega$  phase, as illustrated by the phase diagram in Fig. 8 (Ref 10). Suzuki et al. (Ref 22) reported that this athermal  $\omega$  is formed in the regions close to the  $\alpha'$  martensite phase boundaries. Therefore, the specimens cooled at 50 °C/s and via WQ exhibit retained  $\beta$  and  $\omega$  phases around the acicular  $\alpha'$  phase.

XRD results analysis of the aged specimens after solution treatment at different cooling rates exhibit  $\alpha$ -Ti (ICSD 98-009-9778),  $\beta$ -Ti (ICSD 98-007-6165), and  $\text{Ti}_3\text{Al}$  (ICSD 98-060-9522) phases (Fig. 9). The aged specimens cooled at 50 °C/s and via WQ no longer exhibit the peaks related to the  $\omega$  and  $\alpha'$  phases, while  $\alpha$  and  $\beta$  phase peaks are present after aging, corresponding to  $\alpha + \beta$  lamellae as shown in Fig. 5. Peaks related to  $\text{Ti}_3\text{Al}$  precipitation appear in all specimens, regardless of cooling rate.

The phase fractions that appeared after solution treatment, which was the first stage of STA heat treatment, were calculated (Table 3) based on the OM images (Fig. 4) and XRD analysis (Fig. 7). The specimens cooled at 50 °C/s and via WQ exhibited minimal amounts of  $\alpha_{\text{GB}}$ , as seen during OM analysis, thus the  $\alpha_{\text{GB}}$  phase was not considered in these specimens. However, the specimens cooled at 1 and 10 °C/s clearly exhibited the  $\alpha_{\text{GB}}$  phase, so  $\alpha_{\text{GB}}$  fraction within the  $\alpha_{\text{G}}$  fraction. The  $\alpha_{\text{G}_1}$  phase comprised globular-shaped  $\alpha$  formed during solution treatment process, hence being denoted by 1. The fraction of  $\alpha_{\text{G}_1}$  is the sum of the  $\alpha_{\text{P}}$  and secondary  $\alpha$  ( $\alpha_{\text{S,P}}$ ) formed near  $\alpha_{\text{G}_1}$  during cooling at the end of the solution treatment process. The  $\alpha_{\text{P}}$  phase is the  $\alpha$  phase formed during isothermal holding at 950 °C, and the same amount remains when cooled via WQ. However, cooling at a slower rate leads to coarsening of the  $\alpha_{\text{G}_1}$  phase to form  $\alpha_{\text{S,P}}$ . Secondary  $\alpha$  in the  $\alpha + \beta$  lamellae formed during cooling in the solution treatment process is denoted as  $\alpha_{\text{S}_1,\text{L}}$ . Cooling at 1 and 10 °C/s leads to the formation of  $\alpha + \beta$  lamellae. Further, cooling at 50 °C/s led to the formation of both  $\alpha'$  and  $\alpha + \beta$  lamellae, but the XRD peaks related to  $\alpha'$  and  $\alpha$  were not distinguishable. Thus, so the sum of the  $\alpha_{\text{S}_1,\text{L}}$  and  $\alpha'$  fractions was listed in Table 3. Cooling via WQ led to the formation of  $\alpha'$  without  $\alpha_{\text{S,P}}$  or  $\alpha_{\text{S}_1,\text{L}}$ . The  $\beta$  phase fraction was calculated as the sum of both retained  $\beta$  and lamellar  $\beta$ .

The calculated phase fractions after solution treatment are plotted (Fig. 10a), and effect of cooling rate on the phase changes during cooling after isothermal holding at 950 °C is illustrated (Fig. 10b). The Ti-6Al-4V alloy consisted of  $\sim 80\%$   $\alpha$  and  $\sim 20\%$   $\beta$  before solution treatment, and  $\sim 30\%$   $\alpha$  ( $\alpha_{\text{P}}$ ) and 70%  $\beta$  after being held at 950 °C for 1 h. Cooling from this state via WQ leads to retention of  $\alpha_{\text{P}}$  to constitute  $\alpha_{\text{G}_1}$ , and transformation of  $\beta$  to  $\alpha'$  and  $\omega$ . Cooling at 50 °C/s is slower than WQ, and leads to the addition of a small amount of  $\alpha_{\text{S,P}}$  to  $\alpha_{\text{P}}$ , as well as a slight increase in  $\alpha_{\text{G}_1}$ , and transformation of  $\beta$  to either  $\alpha'$  or  $\alpha + \beta$  lamellae. Further, smaller amount of  $\omega$  phase than in the WQ sample is observed around  $\alpha'$ .

Slower cooling at 1 and 10 °C/s transformed the existing  $\beta$  formed at 950 °C to  $\alpha + \beta$  lamellae, and no  $\alpha'$  and  $\omega$  phases are formed. The  $\alpha_{\text{G}_1}$  formed at 1 °C/s is coarser and the fraction is larger compared to cooling at 10 °C/s (Fig. 4a and b). The amount of  $\alpha_{\text{S,P}}$  was determined by subtracting the amount of  $\alpha_{\text{P}}$  from the amount of  $\alpha_{\text{G}_1}$ , regardless of cooling rate. The amount of  $\alpha_{\text{S,P}}$  increases dramatically after cooling at 1 °C/s compared

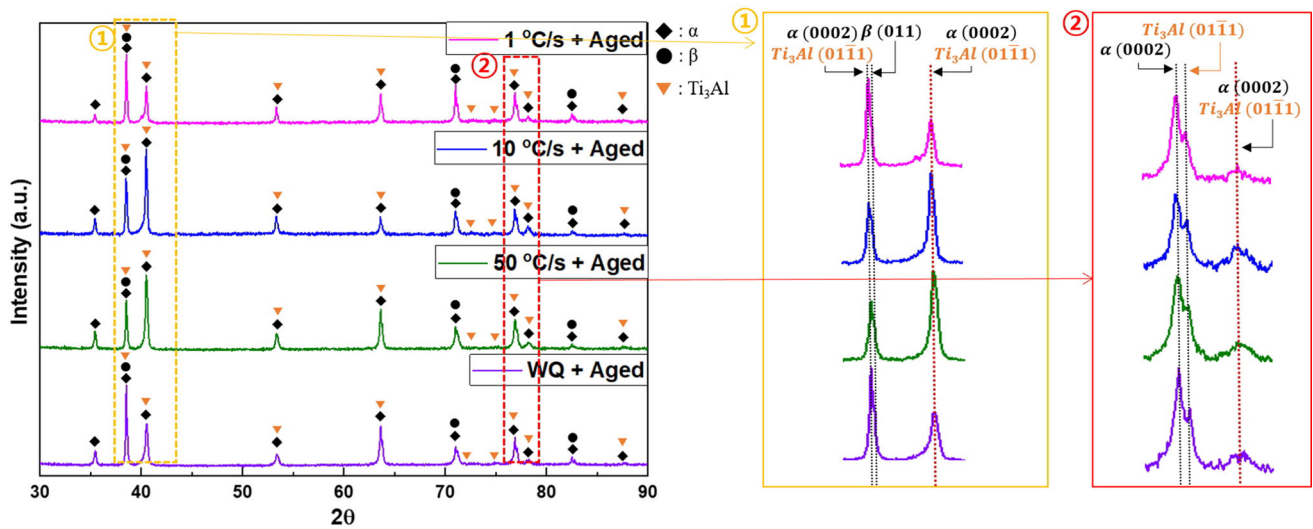


Fig. 9 XRD patterns of Ti-6Al-4V alloys after subsequent aging at 500 °C for 4 h after solution treatment with different cooling rates

Table 3 Phase fractions (%) of Ti-6Al-4V alloys after solution treatment with different cooling rates based on XRD and OM analysis

		1 °C/s	10 °C/s	50 °C/s	WQ
$\alpha_{G1}$	$\alpha_P$	31.88			
	$\alpha_{S,P}$	31.85	2.37	1.92	...
$\alpha_{S1,L}$		20.70	42.31	48.71	...
$\alpha'$		...	...	...	51.64
$\beta$		15.57	23.44	10.45	8.05
$\omega$		...	...	7.04	8.43

The  $\beta$  phase is observed in all specimens, regardless of cooling rate in the solution treatment process. However, cooling via WQ leads to the retention of a small amount of  $\beta$  that was not transformed to  $\alpha'$ . Cooling at 50 °C/s leads to a larger amount of  $\beta$  phase compared to cooling via WQ, which was taken as the sum of the retained  $\beta$  and lamellar  $\beta$  plates. Slower cooling at 1 and 10 °C/s leads to transformation of  $\beta$  to  $\alpha + \beta$  lamellae without transformation to  $\alpha'$ , resulting in a larger amount of  $\beta$  compared to the specimens cooled at 50 °C/s and via WQ. Further, less  $\beta$  to  $\alpha + \beta$  lamellar transformation occurs at 10 °C/s compared to 1 °C/s, leading to a larger amount of  $\beta$  phase.

The phase fractions that appeared after aging, which was the

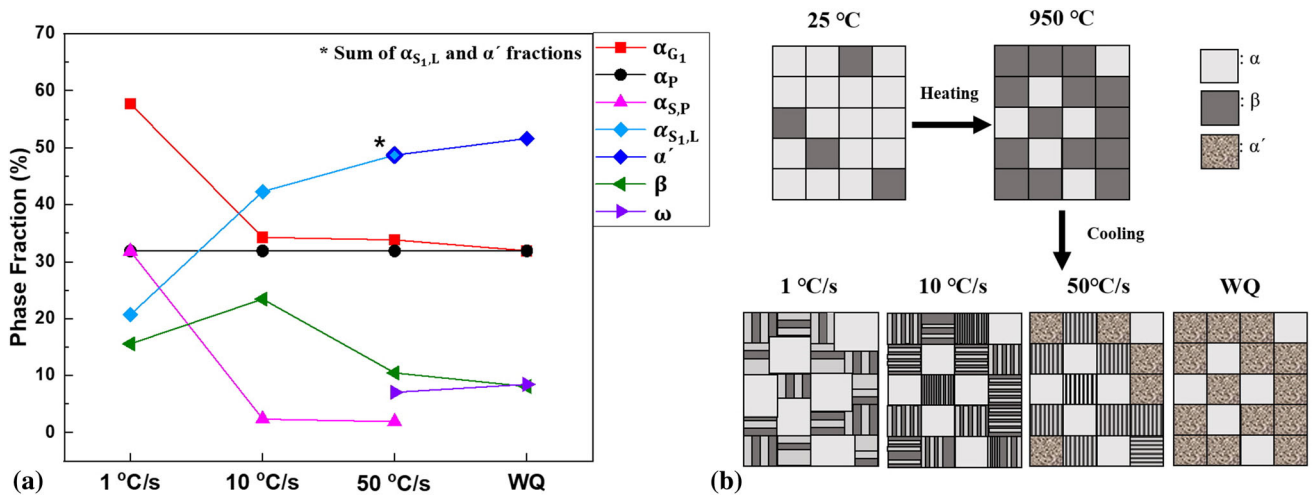


Fig. 10 (a) Calculated phases fractions after solution treatment with different cooling rates and (b) illustration of the effect of cooling rate on the phase changes during solution treatment

to 10 °C/s, while the amount of  $\alpha_{S1,L}$  is significantly reduced. This is attributed to the larger amount of  $\alpha_{S,P}$  formed and grown next to  $\alpha_P$  at the slower cooling rate, as well as the formation of  $\alpha$  from  $\alpha_{GB}$ , and the coarsening of some  $\alpha_{S1,L}$  in a globular form that was considered as  $\alpha_{G1}$ .

second stage of STA heat treatment, were calculated (Table 4) based on the OM images (Fig. 5) and XRD analysis (Fig. 9). The globular  $\alpha$  ( $\alpha_{G2}$ ) formed after aging, and thus denoted by 2, is taken as the sum of  $\alpha_{G1}$  formed after solution treatment and the secondary  $\alpha$  phase ( $\alpha_{S,G1}$ ) formed near  $\alpha_{G1}$  during aging. The  $\alpha$  phase in the  $\alpha + \beta$  lamellae formed from  $\alpha'$  and/or

**Table 4** Phase fractions (%) of Ti-6Al-4V alloys after subsequent aging at 500 °C for 4 h after solution treatment with different cooling rate based on XRD and OM analysis

		1, °C/s	10, °C/s	50, °C/s	WQ
$\alpha_{G_2}$	$\alpha_{G_1}$	53.72-55.12	27.94-30.12	27.17-29.73	25.24-27.87
	$\alpha_{S,G_1}$	6.57-6.73	6.03-6.50	4.62-5.06	4.12-4.54
$\alpha_{S_2,L}$		16.89-17.54	39.57-43.39	40.03-44.71	41.30-46.51
$\beta$		6.99	7.72	8.27	8.47
$Ti_3Al$		13.61-15.83	12.26-18.73	12.23-19.91	12.60-20.87

coarsened  $\alpha_{S_1,L}$  during aging is represented as  $\alpha_{S_2,L}$ . The XRD patterns (Fig. 9) exhibit some of peaks corresponding to  $\alpha$  and  $Ti_3Al$  at the same  $2\theta$ , thus the phase fractions are expressed as a range. The  $\alpha$  phase fraction (Table 4) was determined by subtracting  $Ti_3Al$  from the amount of  $\alpha$  calculated based on the OM and XRD results.  $Ti_3Al$  was entirely precipitated from all of the  $\alpha$  phase, but the accuracy of the precipitation measurements was limited due to the types of  $\alpha$  phases ( $\alpha_{G_1}$ ,  $\alpha_{S,G_1}$ , and  $\alpha_{S_2,L}$ ) formed during the STA process. Thus, the amount of  $Ti_3Al$  precipitates in each  $\alpha$  phase was assumed to be proportional to the amount of each  $\alpha$  phase.

The calculated phase fractions after aging are plotted (Fig. 11a), and the effect of cooling rate on the microstructural changes due to aging are illustrated (Fig. 11b). Overall, the  $\alpha_G$  fraction after aging ( $\alpha_{G_2}$ ) is larger and coarser than that before aging ( $\alpha_{G_1}$ ) (Ref 16). Cooling at 10 °C/s in the solution treatment leads to the transformation of more retained  $\beta$  to  $\alpha$  phase during aging compared to the specimen cooled at 1 °C/s. Thus, the amounts of retained  $\beta$  phase after aging in the specimens cooled at 1 and 10 °C/s are similar, where the amount of retained  $\beta$  phase approaches the equilibrium  $\beta$  phase fraction (5.45 %) at an aging temperature of 500 °C. The specimens cooled at 50 °C/s and via WQ exhibit a larger amount of  $\alpha_{S_2,L}$  after aging compared to cooling at 1 and 10 °C/s due to fine  $\alpha$  plate precipitation and growth.

A slightly larger amount of  $Ti_3Al$  is formed at a faster cooling rate in the solution treatment. Lütjering et al. (Ref 16) reported that the amount of  $\alpha$  stabilizing element in the  $\beta$  phase is smaller than that in the  $\alpha_P$  phase forms during the isothermal holding stage of solution treatment. In addition, the JMatPro

(Ref 20) calculations indicate that less Al is in the equilibrium  $\alpha$  at room temperature compared to that at 950 °C (Fig. 12). Therefore, the  $\alpha$  phase of the  $\alpha + \beta$  lamellar structure forms during slow cooling of the  $\beta$  phase, which is isothermally maintained at high temperature, contained less Al than  $\alpha_G$ . This indicates that less homogeneous nucleation and growth of  $Ti_3Al$  occur in the  $\alpha$  plate inside the lamellar during aging compared to the  $\alpha_G$  phase (Ref 16). However, the amount of Al in the  $\alpha$  phase at different temperatures from 950 °C is relatively insignificant (Fig. 12). Therefore, the finding by Lütjering et al. (Ref 16) that the concentration of Al inside the  $\alpha$  phase leads to a difference in homogeneous nucleation and growth rate of  $Ti_3Al$  is not taken into consideration. However, Zhang et al. (Ref 23) reported that the dislocations and grain boundaries in finer  $\alpha + \beta$  lamellae promote heterogeneous nucleation and growth of  $Ti_3Al$ . The faster cooling rates in this study facilitate transformation  $\beta$  to  $\alpha'$  during solution treatment, which leads to distortion and a high dislocation density. Consequently, the lamellae with fine  $\alpha$  and  $\beta$  plates are decomposed from the  $\alpha'$  phase and contained many grain boundaries after aging (Ref 10). Overall, faster cooling rates in the solution treatment process lead to a higher amount of  $Ti_3Al$  precipitation during aging process due to the dominant effect of the differences in heterogeneous nucleation and growth rate (Ref 23), and not due to the effect of homogeneous nucleation and growth rate (Ref 16).

### 3.3 Effects of $a$ and $a'$ Plate Thickness on Hardness

The plate thickness of the  $\alpha'$  and  $\alpha$  plates in the  $\alpha + \beta$  lamellae produced when cooled at rates of 1, 10, and 50 °C/s

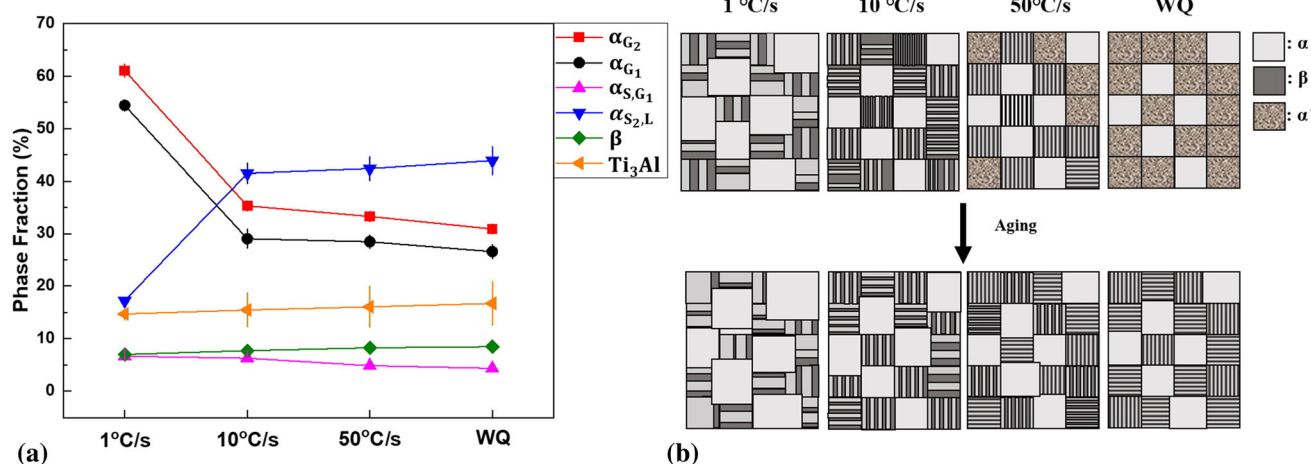


**Fig. 11** (a) Calculated phase fractions after subsequent aging at 500 °C for 4 h after solution treatment with different cooling rates and (b) illustration of the effect of cooling rate on the microstructural changes due to aging



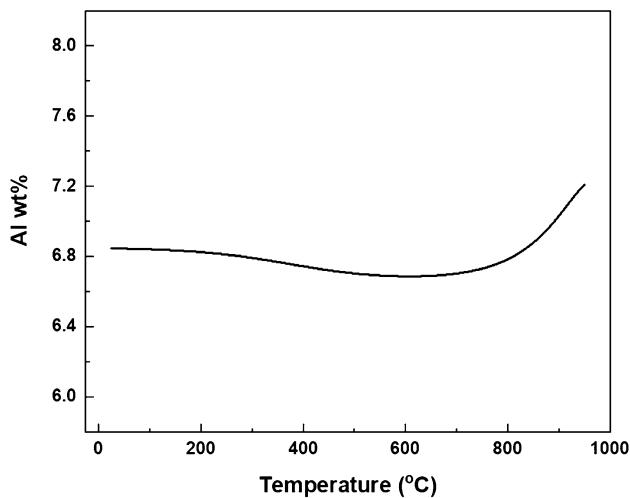


**Fig. 12** Calculated Al concentrations (wt.%) in  $\alpha$  phase at the different heat treatment temperatures

and via WQ was measured before and after aging (Fig. 13a). Specifically, only the  $\alpha$  plates in  $\alpha + \beta$  lamellae were measured for cooling at 1 and 10 °C/s during solution treatment, both the  $\alpha$  and  $\alpha'$  plates were measured for cooling at 50 °C/s, and only the  $\alpha'$  plates were measured for WQ. Cooling at 10 °C/s leads to thinner  $\alpha$  plates in the solution treatment compared to 1 °C/s, while cooling at 50 °C/s leads to thinner  $\alpha$  and  $\alpha'$  plates compared to both 1 and 10 °C/s. WQ, the fastest cooling, leads to the thinnest  $\alpha'$  plates.

The  $\alpha$  plates observed after aging have become coarser and/or were precipitated from  $\alpha'$ . Slower cooling rates in the solution treatment lead to thicker  $\alpha$  plates, where aging of the specimens cooled at 1 and 10 °C/s leads to coarsening of the  $\alpha$  plates formed during cooling, resulting in significant increase in thickness. However, the specimens cooled at 50 °C/s and via WQ exhibit a minimal change in thickness after aging because the fine  $\alpha$  plates are precipitated from  $\alpha'$ .

The hardness (HV) of the specimens before and after aging increases with faster cooling (Fig. 13b). Specifically, the specimen cooled at 10 °C/s exhibits a higher hardness than the specimen cooled at 1 °C/s because thinner  $\alpha$  plates are formed when cooled at 10 °C/s. Unlike cooling at 1 and 10 °C/

s, the specimens cooled at 50 °C/s and via WQ form  $\alpha'$ , which lead to a significant increase in hardness. The fraction of  $\alpha'$  in the WQ sample is higher, thereby leading to a higher hardness value.

The hardness of all specimens increases after aging, where higher hardness values are obtained as the cooling rate of the solution treatment increases. Aging of the specimens cooled at 1 and 10 °C/s leads to a slight increase in hardness just because of the precipitation of  $Ti_3Al$  inside the  $\alpha$  phase (Ref 11). However, aging of the specimens cooled at 50 °C/s and via WQ leads to a substantial increase in hardness due to the precipitation of fine  $\alpha$  from  $\alpha'$  in addition to the precipitation of  $Ti_3Al$ . Therefore, the highest hardness value after aging is obtained with WQ in the solution treatment process.

## 4. Conclusions

The microstructure and hardness of a Ti-6Al-4V alloy sample with a similar size to an aerospace fan disk component were analyzed according to various position-dependent cooling rates (1, 10, and 50 °C/s, and WQ) during STA processing. The following conclusions were obtained:

1. WQ in the solution treatment allows for retention of the globular primary  $\alpha$  phase, and transformation of  $\beta$  to  $\alpha'$ . Controlled cooling (1, 10, and 50 °C/s) slower than WQ leads to coarsening of the globular  $\alpha$  and transformation  $\beta$  to  $\alpha + \beta$  lamellae (In the case of 50 °C/s,  $\beta$  is partially transformed to  $\alpha'$ ). Thicker lamellar plates are formed at slower cooling rates.
2. Aging of the specimens cooled via WQ and at 50 °C/s leads to the transformation of  $\alpha'$  to fine  $\alpha + \beta$  lamellae. The lamellar plate already formed during cooling at 1, 10, and 50 °C/s in solution treatment becomes coarser during aging, which is more apparent at slower cooling rates.  $Ti_3Al$  is precipitated from  $\alpha$  in all specimens regardless of the cooling conditions.
3. Faster cooling at the end of solution treatment leads to higher hardness values due to the formation of thinner  $\alpha$  plates and/or a higher  $\alpha'$  fraction. Aging of the specimens cooled via WQ and at 50 °C/s leads to a rapid increase in hardness due to the precipitation of both fine  $\alpha$  plates

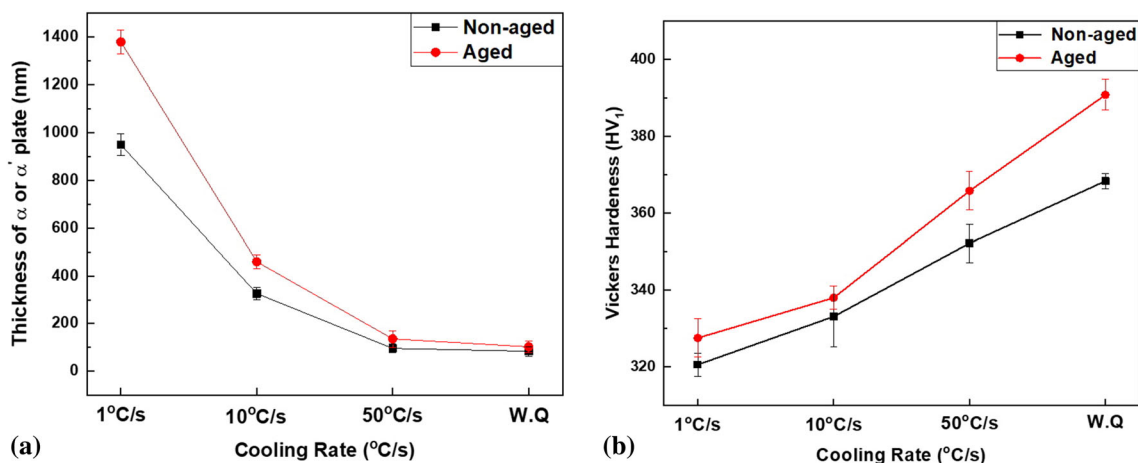


**Fig. 13** (a)  $\alpha$  or  $\alpha'$  plate thickness and (b) Vickers hardness before and after aging with different cooling rates of solution treatment

and Ti<sub>3</sub>Al. However, aging of the specimens cooled at 1 and 10 °C/s leads to a slight increase in hardness only due to Ti<sub>3</sub>Al precipitation.

## Acknowledgments

The authors gratefully acknowledge the extended support provided to this work by the Lightweight Material National Strategy Project (10081335) funded by the Korea Evaluation Institute of Industrial Technology (KEIT).

## References

1. S. Patil, S. Kekade, K. Phapale, S. Jadhav, A. Powar, A. Supare, R. Singh, Effect of  $\alpha$  and  $\beta$  Phase Volume Fraction on Machining Characteristics of Titanium Alloy Ti6Al4V, *Procedia Manuf.*, 2016, **6**, p 63–70
2. L.W. Meyer, L. Krüger, K. Sommer, T. Halle, M. Hockauf, Dynamic Strength and Failure Behavior of Titanium Alloy Ti-6Al-4V for a Variation of Heat Treatments, *Mech. Time-Dependent Mater.*, 2008, **12**(3), p 237–247
3. I. Inagaki, T. Takechi, Y. Shirai, N. Ariyasu, Application and Features of Titanium for the Aerospace Industry, 106, Nippon Steel & Sumitomo metal technical report, Nippon Steel, 2014, p 22–27
4. J. Foltz, ASM handbook volume 4E, G.E. Totten, D.S. Machenzie (eds), Heat Treating of Nonferrous Alloys. ASM International, USA, 2016, Introduction to Titanium and Its Alloys, p 481–497
5. R. Boyer, E.W. Collings, G. Welsch Eds., *Materials Properties Handbook: Titanium Alloys*, ASM International, USA, 1994, p 528–530
6. AMS, Titanium Alloy, 6.0Al-4.0V, Solution Heat Treated and Aged, SAE Specification, 4965m, 2018
7. C. Carson, ASM handbook Volume 4E, G.E. Totten, D.S. Machenzie (eds), Heat Treating of Nonferrous Alloys. ASM International, USA, 2016, Heat treating of Titanium and Titanium alloys, p 511–533
8. A. Gupta, R.K. Khatirkar, A. Kumar, M.S. Parihar, Investigations on the Effect of Heating Temperature and Cooling Rate on Evolution of Microstructure in an  $\alpha + \beta$  Titanium Alloy, *J. Mater. Res.*, 2018, **33**(8), p 946–957
9. M.T. Jovanović, S. Tadić, S. Zec, Z. Mišković, I. Bobić, The Effect of Annealing Temperatures and Cooling Rates on Microstructure and Mechanical Properties of Investment Cast Ti-6Al-4V Alloy, *Mater. Des.*, 2006, **27**(3), p 192–199
10. R. Boyer and J. Foltz, ASM handbook volume 4E, G.E. Totten, D.S. Machenzie (eds), Heat Treating of Nonferrous Alloys. ASM International, USA, 2016, Metallurgy of titanium alloy heat treatment, p 498–509
11. G. Welsch, G. Lütjering, K. Gazioglu, W. Bunk, Deformation Characteristics of Age Hardened Ti-6Al-4V, *Metall. Trans. A*, 1977, **8**(1), p 169–177
12. T. Morita, K. Hatsuoaka, T. Iizuka, K. Kawasaki, Strengthening of Ti-6Al-4V Alloy by Short-Time Duplex Heat Treatment, *Mater. Trans.*, 2005, **46**(7), p 1681–1686
13. S.T. Oh, K.D. Woo, J.H. Kim, S.M. Kwak, Effect of Retained  $\beta$  Phase on Mechanical Properties of Cast Ti-6Al-4V Alloy, *Mater. Trans.*, 2017, **58**(8), p 1145–1149
14. S. Tanaka, T. Morita, K. Shinoda, Effects of Short Time Duplex Heat Treatment on Microstructure and Fatigue Strength of Ti-6Al-4V alloy, *ICF*, 2013, **13**, p 16–21
15. Y.C. Lin, Y. Tang, Y.Q. Jiang, J. Chen, D. Wang, D.G. He, Precipitation of Secondary Phase and Phase Transformation Behavior of a Solution-Treated Ti-6Al-4V Alloy During High-Temperature Aging, *Adv. Eng. Mater.*, 2020, **22**(5), p 1901436
16. G. Lütjering, J.C. Williams, Titanium, 2nd ed., B. Derby (ed.), Springer-Verlag, Berlin, 2007, p 203–215
17. P. Pinke, L. Claplovic, T. Kovacs, The Influence of Heat Treatment on the Microstructure of the Casted Ti6Al4V Titanium Alloy, Slovak University of Technology, Bratislava, Web, p. 11, 2011
18. R.K. Gupta, V.A. Kumar, S. Chhangani, Study on Variants of Solution Treatment and Aging Cycle of Titanium Alloy Ti6Al4V, *J. Mater. Eng. Perform.*, 2016, **25**(4), p 1492–1501
19. Y. Ren, S.M. Zhou, Z.Y. Xue, W.B. Luo, Y.J. Ren, Y.J. Zhang, Effect of  $\alpha$ -Platelet Thickness on the Mechanical Properties of Ti-6Al-4V Alloy with Lamellar Microstructure, *IOP Conf. Ser. Mater. Sci. Eng.*, 2017, **281**(1), p 012024
20. JMaPro version 7.0.0, Sente Software Corp., Guildford, UK, 2012
21. S.J. Oh, I.J. Shon, S.J. Lee, Effect of Milling Time and Addition of PCA on Austenite Stability of Fe-7%Mn Alloy, *J. Korean Powder Metall. Inst.*, 2018, **25**(2), p 126–131
22. T. Suzuki, M. Wuttig, Analogy Between Spinodal Decomposition and Martensitic Transformation, *Acta Metall.*, 1975, **23**(9), p 1069–1076
23. J. Zhang, D. Li, Preferred Precipitation of Ordered  $\alpha_2$  Phase at Dislocations and Boundaries in Near- $\alpha$  Titanium Alloys, *Mater. Sci. Eng.*, 2003, **341**(1–2), p 229–235

**Publisher's Note** Springer Nature remains neutral with regard to jurisdictional claims in published maps and institutional affiliations.